A&A 527, A4 (2011)
DOI: 10.1051/0004-6361/201015819

Astronomy & Astrophysics

Stress polishing of thin shells for adaptive secondary mirrors

Application to the Very Large Telescope deformable secondary

E. Hugot[1], M. Ferrari[1], A. Riccardi[2], M. Xompero[2], G. R. Lemaître[1], R. Arsenault[3], and N. Hubin[3]

[1] Laboratoire d'Astrophysique de Marseille, Centre National de la Recherche Scientifique (CNRS)/Aix Marseille Université, 38 rue F. Joliot Curie, 13388 Marseille Cedex 13, France
e-mail: emmanuel.hugot@oamp.fr
[2] Istituto Nazionale di Astrofisica, Osservatorio Astrofisico di Arcetri, L. go E. Fermi 5, 50125 Firenze, Italy
[3] ESO, European Southern Observatory, Karl-Schwarzschild-Str. 2, 85748 Garching b. München, Germany

Received 24 September 2010 / Accepted 12 November 2010

ABSTRACT

Context. Adaptive secondary mirrors (ASM) are, or will be, key components on all modern telescopes, providing improved seeing conditions or diffraction limited images, thanks to the high-order atmospheric turbulence correction obtained by controlling the shape of a thin mirror. Their development is a key milestone towards future extremely large telescopes (ELT) where this technology is mandatory for successful observations.
Aims. The key point of actual adaptive secondaries technology is the thin glass mirror that acts as a deformable membrane, often aspheric. On 6 m−8 m class telescopes, these are typically 1 m-class with a 2 mm thickness. The optical quality of this shell must be sufficiently good not to degrade the correction, meaning that high spatial frequency errors must be avoided. The innovative method presented here aims at generating aspherical shapes by elastic bending to reach high optical qualities.
Methods. This method is called stress polishing and allows generating aspherical optics of a large amplitude with a simple spherical polishing with a full sized lap applied on a warped blank. The main advantage of this technique is the smooth optical quality obtained, free of high spatial frequency ripples as they are classically caused by subaperture toolmarks. After describing the manufacturing process we developed, our analytical calculations lead to a preliminary definition of the geometry of the blank, which allows a precise bending of the substrate. The finite element analysis (FEA) can be performed to refine this geometry by using an iterative method with a criterion based on the power spectral density of the displacement map of the optical surface.
Results. Considering the specific case of the Very Large Telescope (VLT) deformable secondary mirror (DSM), extensive FEA were performed for the optimisation of the geometry. Results are showing that the warping will not introduce surface errors higher than 0.3 nm rms on the minimal spatial scale considered on the mirror. Simulations of the flattening operation of the shell also demonstrate that the actuators system is able to correct manufacturing surface errors coming from the warping of the blank with a residual error lower than 8 nm rms.

Key words. instrumentation: adaptive optics – instrumentation: high angular resolution

1. Active and adaptive optics

1.1. Adaptive secondary mirrors

Large deformable secondary mirrors (DSM) are a promising solution for the next generation of high-order adaptive optics (AO) systems. These pre-focal systems correct the atmospheric turbulence directly in the telescope to feed all focal stations, and can be used to deliver a diffraction-limited image over a small field (a few arcseconds) or an improved seeing over a larger field (up to 10 arcmin) by correcting the ground-layer turbulence (Arsenault et al. 2004). The use of a DSM reduces the number of optical surfaces used for the atmospheric turbulence correction. There are fundamental advantages to have one mirror of the telescope train be adaptive. The whole telescope then becomes an adaptive optical system, offering fast wavefront correction without the addition of supplementary optics or mechanics. The system gives better throughput to science instruments, lower emissivity for thermal infrared instruments, a large field of view that is accessible to all instruments and less complexity at the focal planes.

This adaptive secondary technology has been pioneered for the Multiple Mirror Telescope (MMT, Mount Hopkins, Arizona), and now this 640 mm diameter – 336 actuators system is fully operational (Lloyd Hart et al. 2000; Brusa et al. 2004). The basic concept is to compensate for the atmospheric turbulence by elastically bending a thin glass shell through an array of voice-coil driven position actuators. The stroke is increased compared to piezoelectric devices (up to 50 μm), but requires a membrane made of a large Zerodur aspheric thin shell used as the mirror surface and attached to the actuators. Two other DSM are under final qualification for the Large Binocular Telescope (LBT, Mount Graham, Arizona), which is 911 mm in diameter and is controlled by 672 actuators. Recent on-sky results presented by Esposito et al. (2010) demonstrated the first extreme adaptive optics correction with a DSM on the LBT, with 82% of Strehl in H band, providing images three times sharper than with the Hubble Space Telescope.

The ESO adaptive optics facility development is presently retrofitting one VLT unit into an adaptive telescope. The VLT DSM unit will be controlled by 1170 voice-coil actuators with a pitch of 28.9 mm, acting on a 1.1 m diameter and 2 mm

Table 1. Parameters of the Zerodur DSMs for MMT, LBT and VLT.

Telescope	MMT	LBT	VLT
Shape	Convex asph	Concave asph	Convex asph
Roc [mm]	1795.0	1974.2	4553.6
Conic constant	–1.409	–0.7328	–1.66926
Diameter [mm]	642	911	1120
Thickness [mm]	2	1.6	2
N actuators	336	672	1170

Notes. Roc = Radius of curvature.

thin Zerodur shell, convex hyperbolic. Preliminary simulations have been performed by Arsenault et al. (2006a) to estimate the potential gains in terms of improved image quality and energy concentration. For a ground layer correction over a large field (8 arcmin), the gain in ensquared energy is a factor 2 in all near infrared wavelengths. This can be compared to a global improvement in terms of seeing. For an on-axis correction, diffraction-limited images will be feasible in the visible (around 750 nm) over a small field of view (10 arcsec). From the technical point of view a complete description of the VLT DSM unit is given by Arsenault et al. (2006b), and Table 1 summarizes the principal parameters of the adaptive secondaries for MMT, LBT and VLT. The success of these developments is considered a key milestone towards future ELTs, where the telescopes themselves must be adaptive to ensure their right functionality (Gilmozzi & Spyromilio 2007).

1.2. Active optics and stress polishing

One of the key points of adaptive secondaries is the manufacturing of the Zerodur shell, with an optical quality sufficiently good not to degrade the performances of the AO correction. The MMT and LBT shells have been polished with the stressed laps technology developed by the *Mirror Lab* (Martin et al. 2000, 2006). We propose here an asphérisation method based on the bending of the mirror itself instead of the lap during polishing with a full sized spherical lap. The specific case of the VLT thin shell manufacturing is used as a detailed application.

This method is called *stress polishing* and is a direct application of Active Optics methods, which aims at controlling the deformations of telescope mirrors to improve the quality of astronomical images. These deformations have several origins; the behaviour of optical substrates depends on the internal and external loads, and on the mechanical characteristics of materials. Active Optics allows controlling the deformations of optical components to obtain complex surfaces of high optical quality, statically or dynamically. Based on the elasticity theory, the parametrization of mirror's deformation allows their control in situ or during their manufacturing, resulting in the following main applications (Lemaitre 2009):

1. large amplitude asphérization of optics by stress polishing and/or by in situ stressing (Everhart 1966; Lubliner & Nelson 1980; Nelson et al. 1980; Sporer 2006; Lemaitre 2005);
2. in situ compensation of large telescope mirrors owing to their deflection in field gravity (Noethe et al. 1988; Wilson 1999);
3. availability of a variable asphericity for telescopes with multiple focii selected by mirror interchanging (Lemaitre et al. 1981, 1989);
4. field compensation and cophasing of optical telescope arrays by variable curvature/astigmatism mirrors, (Ferrari 1998; Hugot et al. 2008);
5. segments and diffraction gratings aspherized by replication techniques from active submasters (Huber et al. 1981).

Since the success of Active Optics at NTT and VLT (Wilson et al. 1987, 1991), the world's largest telescopes have integrated active mirrors in their design, which improves their performance. But the new scientific objectives of the astronomical community from cosmology to exoplanets detection require telescopes and instrumentation with an ever better performance, either for ground-based astronomy or in space. This generation of giant telescopes and instruments needs new developments in terms of technology, performance, and optical surface quality. In this context, they are strongly linked to scientific programmes and new imaging technologies because the Active Optics methods enables the production of complex optical surfaces of very high quality, either in static or dynamic mode. The next generation of astronomical instruments will benefit from the optical quality of active and adaptive components (Cuby et al. 2006).

2. Stress polishing for high-quality aspherics

2.1. Stressed mirror polishing for axisymmetric aspherics

The proposed stress polishing method is derived from Schmidts plate stress polishing (1932). Improved by Lemaître (1972), this technique is able to produce an infinite set of aspheres of radius R_a and conic constant K. Two different back pressures are applied on a plate supported on a ring, producing on the inner part a deflection profile corresponding to the inverse of the desired asphere. Then a spherical or flat polishing is applied to remove the material corresponding to the deflection. After removal of the loads, the plate turns back in its stress-free state and the polished surface becomes aspherical.

The main advantage of this technique is to avoid high spatial frequency (HiF) ripples that are associated with the generation of aspherical surfaces by robotic small tool approaches. The full size tool polishing naturally produces smooth surfaces and does not generate such HiF errors. Minimising HiF errors on the optical surfaces allows for a strong reduction of diffractive effects in the optical train and in this way, a minimisation of residual speckles in the focal plane. This point is a major advantage for scientific goals such as exo-planet detection which requires high-contrast imaging as described by Macintosh et al. (2005), Hinkley et al. (2007), or Soummer et al. (2007).

However, one limitation of the two-zones technique is the loss of material at the edge, outside the supporting ring, which is only used to adjust a specific deflection profile on the internal zone.

We adapt this method to use the quasi full aperture of the blank to be warped, avoiding this loss of material. For that, a specific thickness distribution is machined onto the rear face of the blank. That also allows us to use a single back pressure and reduces the complexity of the system. Figure 1 describes the main steps of the stress polishing process. This improvement requires first an analytical definition of the thickness profile and then a numerical optimisation. The manufacturing error budget must be subdivided to identify each potential source of error (Hugot et al. 2009). In a preliminary approach we can write the total amount of rms surface error σ_e as

$$\sigma_e^2 = \sigma_{def}^2 + \sigma_{sup}^2 + \sigma_{pol}^2 + \sigma_{mes}^2, \quad (1)$$

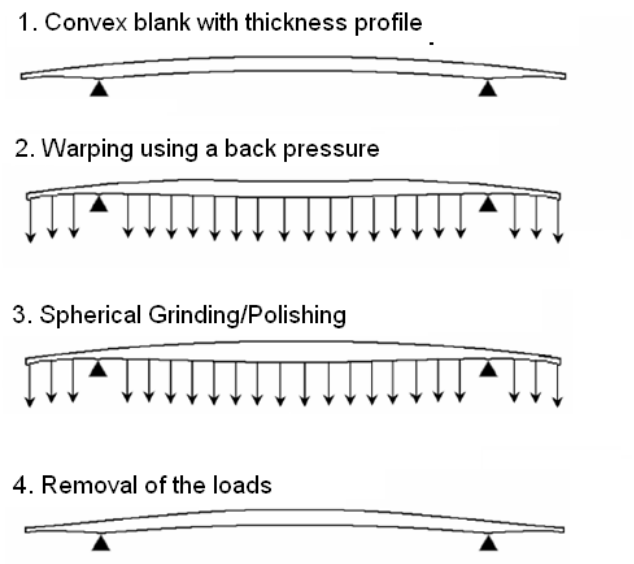

Fig. 1. Description of the Active Optics manufacturing process. 1: A convex blank with radial thickness distribution is supported on a circular ring. 2: The blank is warped into the exact inverse of the final aspherical shape using a back pressure. 3: The spherical grinding/polishing removes the material corresponding to the deformation. 4: After removal of the loads, the blank turns back into its stress-free state and the polished surface becomes aspherical.

where σ_{def} is the surface error from the deflection, σ_{sup} is the surface error generated by the mechanical support during polishing, σ_{pol} is the polishing surface error, and σ_{mes} is the error coming from the test set-up. The first step described here is the minimisation of the deflection errors. In a first approximation we can stand that each term must be lower than $\sigma_e/2$.

2.2. Mirror's bending during polishing

Let uss define a convex spherical surface with a radius of curvature R_s. The optical surface is expressed by

$$Z_s(r) = -R_s + \sqrt{R_s^2 - r^2}. \tag{2}$$

After polishing, the optical surface must be aspherical with a radius of curvature R_a and a conic constant K:

$$Z_a(r) = \frac{1}{1+K}\left(-R_a + \sqrt{R_a^2 - (1+K)r^2}\right). \tag{3}$$

The difference between both surfaces corresponds to the amount of material to be removed during the polishing process. In other words, it corresponds to the flexure Z_{flex} to be applied:

$$Z_a(r) = Z_s(r) - Z_{\text{flex}}(r). \tag{4}$$

Developing expressions of Z_a and Z_s allows rewriting Z_{flex} as:

$$\begin{aligned} Z_{\text{flex}}(r) \;=\; & \frac{1}{2}\left(\frac{1}{R_a} - \frac{1}{R_s}\right)r^2 \\ & + \frac{1}{8}\left(\frac{1+K}{R_a^3} - \frac{1}{R_s^3}\right)r^4 \\ & + \frac{1}{16}\left(\frac{(1+K)^2}{R_a^5} - \frac{1}{R_s^5}\right)r^6 + \dots \end{aligned} \tag{5}$$

From this equation, the elasticity theory will help us to determine the optimal geometry of the mirror to be bent during polishing. A variable thickness distribution on the substrate will allow to reach this deflection, as we show below.

2.3. Variable thickness distribution for precise mirror's bending

The analytical equations coming from the elastic theory of plates (Timoshenko 1959) are leading to a load configuration and a specific thickness distribution. We define below the loadcase and the geometry of the substrate. The proposed solution is applicable to any asphere of radius R_a and conic constant K. Defining cylindrical coordinates (r, θ, Z), the thickness distribution is noted $t(r)$. The problem is axisymmetrical, so that the solution does not depend on the angular coordinate θ.

2.3.1. Elasticity theory

The mirror is modelled with a circular thin plate with parallel faces in the (r, θ) plane. Its external radius is denoted r_e, its thickness t. This plate is simply supported on a ring of radius r_i ($r_i < r_e$), and a uniform load q is applied on its rear face. The plate has an elastic behaviour characterised by its Young's modulus E and its Poisson's ratio ν. The rigidity of the plate D is

$$D = \frac{Et^3}{12(1-\nu^2)}. \tag{6}$$

Denoting with w the radial flexure of the plate, the slope of the flexion is

$$\varphi = \frac{\mathrm{d}}{\mathrm{d}r}w. \tag{7}$$

The moment tensor $\underline{M}$ is a function of the slope φ

$$\underline{M} = D\begin{pmatrix} \frac{\mathrm{d}}{\mathrm{d}r}\varphi + \frac{\nu}{r}\varphi & 0 \\ 0 & \nu\frac{\mathrm{d}}{\mathrm{d}r}\varphi + \frac{1}{r}\varphi \end{pmatrix}_{(r,\theta)}. \tag{8}$$

Denoting Q the shearing force by unit of length, relative to the load q, the equilibrium equation of an elementary section of the plate is

$$M_{rr}(r) + r\frac{\mathrm{d}}{\mathrm{d}r}M_{rr}(r) - M_{\theta\theta}(r) + Q(r)r = 0. \tag{9}$$

From the expression of Z_{flex}, we express the radial moment M_{rr} as a function of r

$$\begin{aligned} M_{rr}(r) \;=\; & D\left[(1+\nu)\left(\frac{1}{R_a} - \frac{1}{R_s}\right)\right. \\ & + \frac{1}{2}(3+\nu)\left(\frac{1+K}{R_a^3} - \frac{1}{R_s^3}\right)r^2 \\ & \left. + \frac{3}{8}(5+\nu)\left(\frac{(1+K)^2}{R_a^5} - \frac{1}{R_s^5}\right)r^4\right]. \end{aligned} \tag{10}$$

2.3.2. Deflection of the internal zone

The plate is simply supported on a radius $r = r_i$, under a uniform load q. Its deflection on $0 < r < r_i$ is denoted w. For constant thickness, we will determine q in order to obtain a deflection

w corresponding to Z_{flex}. The configuration of the internal zone of the plate could be described as a simply supported plate on $r = r_{\text{i}}$, under a uniform load q and a flexure moment $M_{r_{\text{i}}}$ on $r = r_{\text{i}}$, with $M_{r_{\text{i}}} = -M_{rr}(r_{\text{i}})$. The deflection w is the superposition of the deflections corresponding to the two loadcases

$$w(r) = \frac{q}{64D}\left(\frac{5+\nu}{1+\nu}r_{\text{i}}^2 - r^2\right)(r_{\text{i}}^2 - r^2) - \frac{M_{r_{\text{i}}}}{2D(1+\nu)}(r_{\text{i}}^2 - r^2). \quad (11)$$

Writing the deflection like $w(r) = C_4 r^4 + C_2 r^2 + C_0$ allows us to adjust the ratio C_4/C_2 using the parameter q to obtain a deflection w corresponding to Z_{flex}. However, we can neglect the r^6 term and high-order terms if the error introduced by this approximation does not degrade the optical quality of the deflection compared to the specifications, i.e. if $\sigma_{\text{def}} < \sigma_{\text{e}}/2$ in Eq. (1).

2.3.3. Calculation of the load q

Except for the case $r = 0$, the slope of Z_{flex} is equal to 0 on a radius denoted r_{tg}, depending on the aspherical shape desired. We wish to obtain a load q for which $\left.\frac{\mathrm{d}w}{\mathrm{d}r}\right|_{r_{\text{tg}}} = 0$. Using Eq. (11), this condition gives

$$q = \frac{16 M_{r_{\text{i}}}}{(3+\nu)r_{\text{i}}^2 - 2(1+\nu)r_{\text{tg}}^2}. \quad (12)$$

2.3.4. Elastic solution for the external zone

We wish to define a radial thickness distribution $t(r)$ allowing us to obtain a deflection corresponding to $Z_{\text{flex}}(r)$, when the plate is under the same load q obtained from Eq. (12). The rigidity D is a function of r, so the equilibrium equation (Eq. (9)) can be written as a function of the reduced variable $\rho = r/r_{\text{i}}$. We obtain the following differential equation of the rigidity

$$\left[\frac{\mathrm{d}}{\mathrm{d}\rho}\varphi(\rho) + \frac{\nu}{\rho}\varphi(\rho)\right]\frac{\mathrm{d}}{\mathrm{d}\rho}D(\rho) + \frac{\mathrm{d}}{\mathrm{d}\rho}\left[\frac{\mathrm{d}}{\mathrm{d}\rho}\varphi(\rho) + \frac{1}{\rho}\varphi(\rho)\right]D(\rho) = -Q(\rho)r_{\text{i}}^2. \quad (13)$$

The solution of this equation is the superposition of the general solution of the homogeneous equation and a particular solution

$$D(\rho) = \mathrm{e}^{F(\rho)}\left(k + \int \frac{c(\rho)}{a(\rho)}\mathrm{e}^{-F(\rho)}\mathrm{d}\rho\right), \quad k \in \mathbb{R}, \quad (14)$$

with

$$F(\rho) = -\int \frac{b(\rho)}{a(\rho)}\mathrm{d}\rho, \quad (15)$$

where coefficients a, b, and c are

$$\begin{cases} a(\rho) = \dfrac{\mathrm{d}}{\mathrm{d}\rho}\varphi(\rho) + \dfrac{\nu}{\rho}\varphi(\rho), \\ b(\rho) = \dfrac{\mathrm{d}}{\mathrm{d}\rho}\left[\dfrac{\mathrm{d}}{\mathrm{d}\rho}\varphi(\rho) + \dfrac{1}{\rho}\varphi(\rho)\right], \\ c(\rho) = -Q(\rho)r_{\text{i}}^2. \end{cases} \quad (16)$$

The expression of $Q(\rho)$ on the external zone of the plate is obtained from the equilibrium equation

$$2\pi Q(r)r = \pi r^2 q - \pi r_{\text{i}}^2 q - \pi(r_{\text{e}}^2 - r_{\text{i}}^2)q, \quad (17)$$

which leads to the shearing force expression

$$Q(\rho) = \frac{1}{2}q r_{\text{i}}\left(\rho - \frac{\rho_{\text{e}}^2}{\rho}\right), \quad \rho_{\text{e}} = \frac{r_{\text{e}}}{r_{\text{i}}}. \quad (18)$$

The general solution D_{g} of the homogeneous equation is obtained after integration of $F(\rho)$

$$D_{\text{g}}(\rho) = \frac{k}{|\rho^2 - X_1|^{\frac{\alpha}{2A'_5}}|\rho^2 - X_2|^{\frac{\gamma}{2A'_5}}}, \quad k \in \mathbb{R}, \quad (19)$$

with the following constants

$$\begin{cases} X_1 = -\dfrac{1}{2A'_5}\left(A'_3 - \sqrt{A'^2_3 - 4A'_5A'_1}\right), \\ X_2 = -\dfrac{1}{2A'_5}\left(A'_3 + \sqrt{A'^2_3 - 4A'_5A'_1}\right), \\ \alpha = 24\dfrac{A'_5}{5+\nu} - \gamma, \\ \gamma = \dfrac{24\dfrac{A'_5}{(5+\nu)}X_2 + 8\dfrac{A'_3}{(3+\nu)}}{X2 - X1}, \end{cases} \quad (20)$$

and

$$\begin{cases} A'_1 = \left(\dfrac{1}{R_{\text{a}}} - \dfrac{1}{R_{\text{s}}}\right)(1+\nu)r_{\text{i}}, \\ A'_3 = \dfrac{1}{2}\left(\dfrac{1+K}{R_{\text{a}}^3} - \dfrac{1}{R_{\text{s}}^3}\right)(3+\nu)r_{\text{i}}^3, \\ A'_5 = \dfrac{3}{8}\left(\dfrac{(1+K)^2}{R_{\text{a}}^5} - \dfrac{1}{R_{\text{s}}^5}\right)(5+\nu)r_{\text{i}}^5. \end{cases} \quad (21)$$

The particular solution D_{p} of the differential equation with the second member is

$$D_{\text{p}}(\rho) = \frac{1}{|\rho^2 - X_1|^{\frac{\alpha}{2A'_5}}|\rho^2 - X_2|^{\frac{\gamma}{2A'_5}}} \times \int -\frac{1}{2}q r_{\text{i}}^3\left(\rho - \frac{\rho_{\text{e}}^2}{\rho}\right)\frac{|\rho^2 - X_1|^{\frac{\alpha}{2A'_5}}|\rho^2 - X_2|^{\frac{\gamma}{2A'_5}}}{A'_1 + A'_3\rho^2 + A'_5\rho^4}\mathrm{d}\rho. \quad (22)$$

This integral could be numerically solved. Finally, the thickness distribution is obtained after replacing t by $t(\rho)$ in Eq. (6). We express t as a function of $D(\rho)$

$$t(\rho) = \left[\frac{12(1-\nu^2)}{E}D(\rho)\right]^{\frac{1}{3}}, \quad D(\rho) \geq 0. \quad (23)$$

3. Polishing the VLT-DSM thin shell

3.1. DSM requirements for thin shell surface quality

The polishing errors on the VLT-DSM thin shell can be partially corrected by the 1170 actuators glued onto its back face. One tenth of the actuator performance is dedicated to this operation which is called *flattening*. Thanks to that, the error budget in the thin shell polishing is directly impacted, and specifications in terms of optical quality are relaxed on low spatial frequency (LoF) surface errors. However, the flattening of the shell is limited by three main parameters:

1. the force required for the flattening is limited to 1/10th of the total actuator force, limiting the heat dissipation and the lost in actuator stroke;
2. the polishing errors on high spatial frequency (HiF), corresponding to spatial scale lower than the Nyquist limit (twice the inter-actuator distance) must not limit the overall performances of the AO system in optimal seeing conditions;
3. the correction of LoF generates HiF residual harmonics, called *flattening print through* effect, which must not limit the AO system performances.

A complete study of the impact of the manufacturing optical quality on the system efficiency has been performed: after compensating the manufacturing errors, the optical quality of the VLT DSM must be lower than 9.6 nm rms, a value corresponding to the AO fitting-error residual in the best seeing conditions (seeing 0.21 arcsec, $r_0 = 0.5$ m, $\lambda = 0.5$ μm) (Riccardi 2006). The analytical calculations are based on a simplified model of the thin shell, considering a flat 2 mm shell of infinite diameter. Even if this model does not take into account the shell effect and the edges effect, it leads to a realistic specification in the form of a PSD envelope of allowed surface errors. This envelope is a function of the spatial frequency $k = 2\pi/d$ in [rad]/[m], where d is the considered scale on the mirror

$$\mathrm{PSD}(k) = \begin{cases} \mathrm{PSD}(k_L)\left(\dfrac{k_L}{k}\right) & \text{if} \quad k < k_L = \dfrac{2\pi}{L} \\ \min\left[0.111\dfrac{f_{\max}^2}{\mathcal{D}^2 l^3}\dfrac{1}{k^9}, 0.122\dfrac{(k_0-k)^{13/3}}{k^8}\dfrac{\lambda^2}{(r_0/c)^{5/3}}\right] & \\ \qquad\qquad \text{if} \quad k \in W_{0,0}, k \geqslant k_L & \\ 0.122\dfrac{1}{k^{11/3}}\dfrac{\lambda^2}{(r_0/c)^{5/3}} \quad \text{if} \quad k \ni W_{0,0}, & \end{cases} \tag{24}$$

where $f_{\max}$ is the maximal force used for the flattening, $\mathcal{D}$ the rigidity of the shell, l the inter-actuator pitch, L the limiting scale on the mirror, λ the wavelength, r_0 the seeing parameter, c the scale factor between the primary and the secondary mirror of the telescope and $W_{0,0}$ the Nyquist domain defined by

$$W_{0,0} : |k_x| < k_0/2, |k_y| < k_0/2, \quad k_0 = 2\pi/l. \tag{25}$$

The resulting specification is given in Fig. 2, showing the allowed surface error in terms of their PSD. This power specification is linked to the rms allowed surface error by the relation

$$\sigma_e^2(d) = \frac{1}{2\pi}\int_{\frac{2\pi}{d}}^{\infty} \mathrm{PSD}(k) 2\pi k \mathrm{d}k, \tag{26}$$

plotted in Fig. 3. One can notice that the specification on low spatial frequencies is quite loose, up to 20 μm rms, but very tight on high spatial frequencies, down to 4 nm rms for $d = 20$ mm. Given this very difficult specification on the high spatial frequency errors that is required on such a large piece, the stress polishing technique appears as a particularly appropriate manufacturing method.

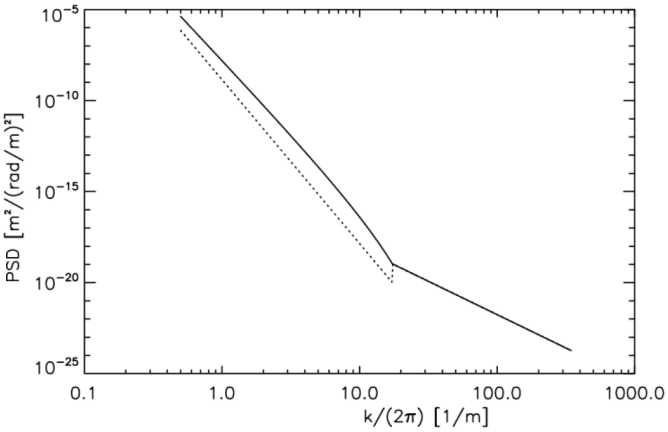

Fig. 2. Envelope of the figuring error PSD for VLT DSM to avoid that the flattening residuals limit the performance of the AO correction with 0.21 arcsec seeing of the PSD of the allowed figuring error. The dashed curve is the PSD envelope taking in account the limitations on the maximum force that can be used to flatten the figuring error.

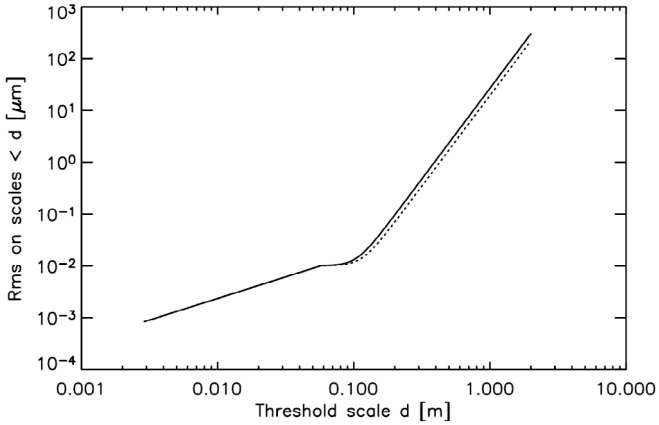

Fig. 3. Maximum rms-figuring error integrated over the range of spatial scales as a function of d for the VLT DSM. The solid and dashed lines represent the 2.0 mm and 1.8 mm thickness case respectively.

3.2. Variable thickness distribution for the VLT thin shell

The VLT deformable secondary mirror will be a Zerodur convex thin shell with the same optical parameters than as existing M2 given in Table 1. The radius of the best-fit sphere (BFS) minimising the rms deviation of this asphere is equal to $R_s = 4575.31$ mm. The mechanical parameters for the Zerodur at room temperature are the Young modulus $E = 90\,600$ MPa and the Poisson ratio $\nu = 0.243$. In order to avoid edge effects during polishing, the total diameter of the mirror must slightly exceed the final one. A preliminary estimate based on our experience leads to a diameter of 1150 mm. The first elasticity calculations are based on this value.

For the internal zone, the thickness is considered as constant. Using Eq. (12), we can calculate the load q function of this thickness for a given supporting radius r_i. This value is fixed by the

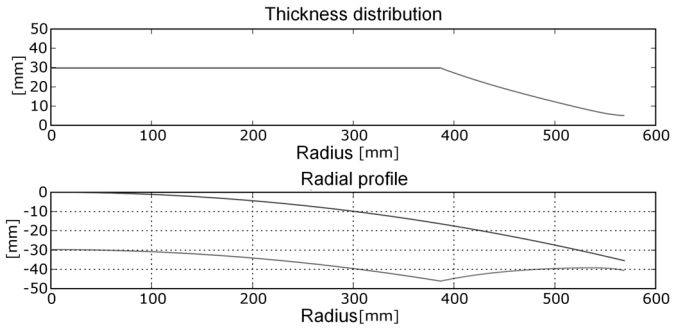

Fig. 4. *Top*: variable thickness distribution on a radius. *Bottom*: profile taking into account the convex shape of the optical surface.

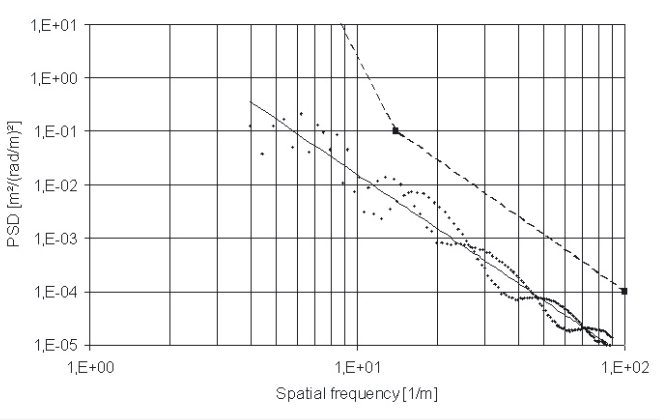

Fig. 5. Power spectral density of the deflection errors compared to the specification. Dashed curve: specification corresponding to Fig. 2. Dotted curve: PSD of the deflection errors obtained from FEA. Plain curve: fitting of dotted curve. With a margin of one decade compared to the specification, the deflection errors will be fully compensated by the actuators.

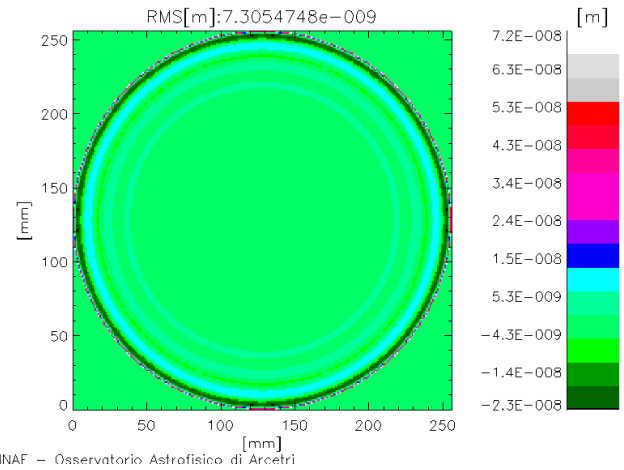

Fig. 6. Flattening residuals. The rms value after flattening of the deflection function errors is lower than 8 nm rms, which validates the thickness profile FEA optimisation.

external diameter of the piece. For a thickness of 30 mm, we get a back pressure equal to 0.3 bars. The parameters fixed from the internal zone study allow the calculation of the variable thickness distribution for the external zone. Using Eq. (23), we find the thickness profile plotted in Fig. 4.

However, analytical calculations just give preliminary definition of the blank's geometry that must be optimised using FEA.

3.3. Flattening the manufacturing errors – finite element validation

Analytical calculations are helpful for a preliminary definition of the blank's geometry but do not take into account several mechanical details in the real design of the mirror. To optimise this preliminary geometry, we perform FEA using Marc/Mentat software. Several details are added to the geometry in order to facilitate the blank machining and to avoid any stress concentration. For instance, the supporting condition on $r = r_i$ is not realised on a radius but on a small annular surface to avoid infinite stress at this location, but this modification will have a significant impact on the optical quality of the deflection. In the same way, the shell effects owing to the curvature of the mirror are not taken into account with the theory of plates. The impacts of these effects have to be characterised by FEA, and then reduced to ensure that $\sigma_{def} < \sigma_e/2$ in Eq. (1).

A specific routine was used to close a loop on the geometrical parameters of the FEA model, with a criterion based on the optical quality of the mechanical deflection. Numerical links between the FEA and interferometry are used to calculate the optical path differences (OPD) map corresponding to the mechanical displacements of the convex face. Results presented in this section were obtained after optimisation of the thickness profile.

The FEA model is axisymmetric and made of 60 067 quadratical quadrangle elements, i.e. a total of 182 582 nodes on a semi-section of the blank, as plotted in Fig. 4 bottom. This meshing corresponds to a sampling of 280 nodes on the optical radius. That gives a Nyquist limit of 4 mm, and a sampling of 10 nodes for the lowest spatial scales in the specification (20 mm). As the substrate is made of Zerodur, a critical point to be checked is the level of stress within the material. The maximal Von Mises stress value obtained after deflection is lower than 2 MPa, which means the material is working down to its statistical elastic limit (8−10 MPa after Schott technical information 2004).

The procedure used is divided in three main steps. The mechanical displacements of the optical surface are calculated on a radius with an axisymmetrical FEA. From that, a 2-dimensional map is generated to get a phase map over a circular aperture. That allows a data reduction using an interferometric software (Intelliwave). The azimuthal average of the 2D-PSD of this map is then compared to the specification and the thickness profile is modified if necessary. The PSD profile obtained after optimisation is plotted in Fig. 5 with $\sigma_{def} < \sigma_e/10$. With a margin of one decade, it is clear that the deflection errors will not introduce high spatial frequency errors. This result now relaxes the allocated error budget on other contributors, which will be helpful for the polishing and testing phases.

The last step for the validation is the fitting error analysis, performed to evaluate the functionality of the shell calculated beyond. The goal is to demonstrate by FEA that the VLT DSM actuators system is able to flatten the manufacturing errors caused by deflection. For that, FEA was performed to quantify the influence functions related to the actuators system, and numerically define the modal basis of the DSM (Riccardi et al. 2006). This model includes the effect of the central membrane and the correct interfaces between magnets and shell, so that it is close to the real behaviour of the DSM.

This modal basis is then used to compute the flattening of the manufacturing error phase map. Results are drawn in Fig. 6 to

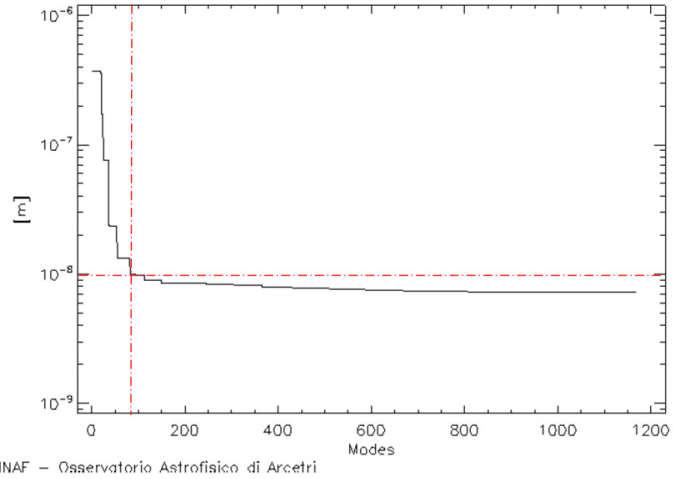

Fig. 7. Flattening residual versus number of corrected modes. Dotted lines show that the 9.6 nm threshold is reached after correcting only 85 modes instead of 1176.

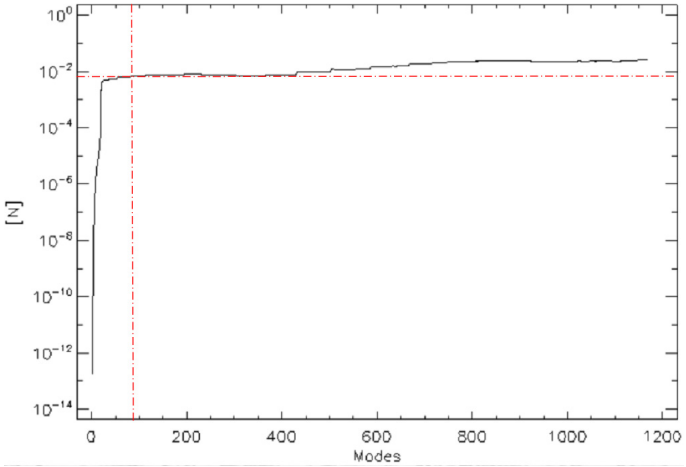

Fig. 8. Rms force versus number of corrected modes. This curve shows that the maximal force used for the flattening of the deflection function errors is lower than 0.025N, below the 0.1N specification. Dotted lines illustrate the force needed to correct the first 85 modes.

show that the flattening residuals are lower than the 9.6 nm rms specification, with a value of 7.3 nm rms. The 9.6 nm threshold is reached after correction of only 85 modes instead of 1176. Figures 7 and 8 indicate that the residual error rapidly decreases after correction of the first 150 modes and then decreases more slowly. The maximal force needed to flatten the mirror is equal to 0.0267N i.e. 1/4 of the specification. All these promising results confirm that the process is suitable for production of the VLT-DSM aspheric convex surface.

4. Conclusions

The stress polishing of aspherics will enable the optimal performances of future adaptive secondaries on 8 m class telescopes, by providing optical surfaces free of high spatial frequency ripples owing to subaperture tool marks. Based on this method, a complete manufacturing process was described. The stress polishing method for producing Schmidt's plates was improved to reduce the complexity of the manufacturing process and also to minimise the loss of material at the edge. The theory of plates has led to a variable thickness distribution, function of the radius of curvature and the conic constant. In the frame of the ESO AO facility development, this method was adapted to the aspherisation of the VLT DSM thin shell. Finite element analysis were performed to optimise this variable thickness distribution and ensure that the actuators system is able to compensate for the surface errors caused by the mechanical deflection errors. We numerically demonstrate that the Active Optics technique based on stress polishing is able to provide an aspherical surface corresponding to the shape of the actual VLT M2. Stress within the material is less than the breakage limit. The deflection does not introduce surface errors that are not compensable by the 1170 actuators. The flattening of the shell reduces the surface error to 7.3 nm rms. The proposed technique is numerically validated, and the next step will be the realisation of the correct optical surface of the VLT DSM by stress polishing at the *Laboratoire d'Astrophysique de Marseille*.

Acknowledgements. This work has been supported by European funding FP6 OPTICON contract CT-2004-001566, *Région PACA*, and *Société européenne des systèmes optiques* (SESO) grant.

References

Arsenault, R., Hubin, N., Le Louarn, M., Monnet, G., & Sarazin, M. 2004, The Messenger, 115, 11
Arsenault, R., Hubin, N., Stroebele, S., et al. 2006a, The Messenger 123, 6
Arsenault, R., Biasi, R., Gallieni, D., et al. 2006b, Proc. SPIE, 6272, 62720V
Brusa, G., Miller, D. L., Kenworthy, M., Fisher, D., & Riccardi, A. 2004, Proc. SPIE, 5490, 23
Cuby, J. G., Prieto, E., Ferrari, M., et al. 2006, Proc. SPIE, 6269, 62691U
Dohlen, K., Beuzit, J. L., & Feldt, M. 2006, Proc. SPIE, 6269, 6269OQ
Everhart, E. 1966, Appl. Opt., 5, 713
Esposito, S., et al. 2010, Proc. SPIE, 7736, 77363H
Ferrari, M. 1998, A&AS, 128, 221
Gilmozzi, R., & Spyromilio, J. 2007, The European Extremely Large Telescope (E-ELT), The Messenger 127, 15
Hinkley, S., Oppenheimer, B. R., Soummer, R., et al. 2007, ApJ, 654, 633
Huber, M. C. E., Jannitti, E., Lemaitre, G. R., & Tondello, G. 1981, Appl. Opt., 20, 2139
Hugot, E., Lemaitre, G. R., & Ferrari, M. 2008, Appl. Opt., 47, 10, 1401
Hugot, E., Ferrari, M., El Hadi, K., et al. 2009, Appl. Opt., 48, 15, 2932
Lemaitre, G. R. 1972, Appl. Opt., 11, 7, 1630
Lemaitre, G. R. 1981, Current trends in optics, International commission for optics 12 (Taylor & Francis London), 135
Lemaitre, G. R. 1989, Proc. SPIE, 1114, 328
Lemaitre, G. R. 2009, Astronomical Optics and Elasticity – Active Optics Methods, 130 (Berlin: Springer)
Lemaitre, G. R., Montiel, P., Joulié, P., Dohlen, K., & Lanzoni, P. 2005, Appl. Opt., 44, 34, 7322
Lloyd-Hart, M., Wildi, F., Martin, H., et al. 2000, Proc. SPIE, 4007, 270
Lubliner, J., & Nelson, J. E. 1980, Appl. Opt., 19, 14, 2332
Macintosh, B., Poyneer, L., Sivaramakrishnan, A., & Marois, C. 2005, Proc. SPIE, 5903, 5903OJ
Martin, H. M., Burge, J. H., Del Vecchio, C., et al. 2000, Proc. SPIE, 4007, 502
Martin, H. M., Brusa, G., Cuerden, B., et al. 2006, Proc. SPIE, 6272, 62720U
Nelson, J., Gabor, G., Hunt, L. K., Lubliner, J., & Mast, T. S. 1980, Appl. Opt., 19, 14, 2341
Noethe, L., Franza, F., & Giordano, P. 1988, J. Mod. Opt., 35, 9, 1427
Riccardi, A. 2006, Proc. SPIE, 6272, 62725O
Riccardi, A., Xompero, M., & Busoni, L. 2006, Proc. SPIE, 6272, 62724O
Schmidt, B. 1932, A coma-free telescope, Mitt Hamburg Strenv., 7, 15
SCHOTT 2004, Technical information TIE, 31
Soummer, R. 2007, ApJ, 669, 642
Sporer, S. F. 2006, Proc. SPIE, 62672R
Timoshenko, S. P., & Woinovsky-Krieger, S. 1959, Theory of Plates and Shells (McGraw-Hill Co.)
Wilson, R. N. 1991, Contemp. Phys., 32, 157
Wilson, R. N. 1999, Reflecting Telescope Optics II (Berlin: Springer), 274
Wilson, R. N., Franza, F., & Noethe, L. 1987, J. Mod. Opt., 34, 485